Research Square

Preprints are preliminary reports that have not undergone peer review.
They should not be considered conclusive, used to inform clinical practice,
or referenced by the media as validated information.

Uracil-DNA glycosylase 1 mitigates acute kidney injury inflammation by maintaining mtDNA homeostasis

Liao xiaohui

lxh@hospital.cqmu.edu.cn

The Second Affiliated Hospital, Chongqing Medical University https://orcid.org/0000-0002-2329-0456

Chunxia Wang

The Second Affiliated Hospital, Chongqing Medical University

Wei Tang

The Second Affiliated Hospital, Chongqing Medical University

Pan Xie

The Second Affiliated Hospital, Chongqing Medical University

Yuting Wang

The Second Affiliated Hospital, Chongqing Medical University

Shan Yang

The Second Affiliated Hospital, Chongqing Medical University

Pengfei Yang

The Second Affiliated Hospital, Chongqing Medical University

Guiquan Yu

The Second Affiliated Hospital, Chongqing Medical University

Zheng Zhang

Chongqing Medical University https://orcid.org/0000-0002-0062-517X

Article

Keywords: Acute kidney injury, UNG1, inflammation, mtDNA, SSBP1

Posted Date: August 28th, 2026

DOI: https://doi.org/10.21203/rs.3.rs-10469724/v1

License: This work is licensed under a Creative Commons Attribution 4.0 International License.
Read Full License

Additional Declarations: There is no conflict of interest

Abstract

Acute kidney injury (AKI) is a common clinical syndrome that is caused by multiple factors, such as ischemia-reperfusion and nephrotoxic drugs. Current treatment strategies for AKI are focused on supportive therapy, and thus, there remains a lack of effective etiological therapies. Mitochondrial dysfunction, which leads to mitochondrial DNA (mtDNA) breaks and triggers cGAS-STING inflammatory responses, has been shown to play a significant role in the progression of AKI. Here, we observed a reduced inflammatory response during AKI in Sting-/- mice prompting us to examine the role of mtDNA in inflammation further. The mitochondrial protein Uracil-DNA glycosylase 1 (UNG1) is a key component of mtDNA base excision repair (BER) and maintains mitochondrial genome stability. Recent studies have shown that UNG-mediated BER is associated with various diseases; however, the role of UNG1 in kidney disease remains under-reported. In this study, we confirmed mitochondrial dysfunction in both in vivo and in vitro models of AKI and identified a mtDNA-mediated inflammatory response. Our results indicate that overexpression of UNG1 in mice significantly alleviates renal dysfunction and inflammatory responses induced by ischemia-reperfusion and cisplatin. Concurrently, overexpression of UNG1 in cells was found to reduce mtDNA breaks and leakage, and attenuated mtDNA-mediated inflammatory responses. Through mass spectrometry, we identified a potential binding interaction between the mtDNA nucleoid-associated protein single-stranded DNA binding protein 1 (SSBP1) and UNG1. This binding affinity was confirmed through molecular docking, and Co-IP. In addition, using oligomerization assays, we showed that UNG1 promoted SSBP1 dimer/tetramer formation, while ChIP assays further verified that UNG1 regulated SSBP1-mtDNA binding. Finally, the protective effects of UNG1 were also observed in AKI Sting-/- mice. In conclusion, our study shows that UNG1 effectively alleviates AKI by promoting SSBP1-mediated nucleoid formation, suggesting that UNG1 may be a potential therapeutic target for managing and treating AKI.

Introduction

Acute kidney injury (AKI) is a common clinical syndrome characterized by a sudden loss of kidney function that occurs over several hours to seven days.[1] AKI episodes are associated not only with short-term adverse outcomes but also with long-term detrimental effects on survival, contributing to significant morbidity, mortality, and healthcare burden.[2] Common causes include nephrotoxin exposure, ischemia/reperfusion (I/R) injury, sepsis, and obstructive insults.[3] Currently, early diagnosis of AKI remains a formidable challenge, with specific and effective therapies unable to meet clinical demand.[4] Therefore, there is an urgent need to elucidate the pathogenesis of AKI.

Renal tubular epithelial cells (RTECs) are the primary intrinsic cell type in the kidney. Since proximal tubulars are directly exposed to toxic filtrate and highly metabolically active, they are rich in mitochondria but highly susceptible during AKI.[5, 6] RTECs are adaptive to mild injury and RTEC regeneration leads to the restoration of tubular integrity. However, when suffering persistent or severe injury, these regenerative processes become dysregulated leading to chronic renal dysfunction.[7, 8] Many studies

have reported that inflammation is a crucial cause of maladaptive RTEC repair and the development of AKI.[9, 10] Mitochondrial DNA (mtDNA) encodes 13 proteins associated with the oxidative phosphorylation system. mtDNA is vulnerable to oxidative stress due to its lack of histones and close proximity to the electron transport chain.[11] Damaged mtDNA not only results in mitochondrial dysfunction but is also released into the cytoplasm, where cytosolic mtDNA fragments subsequently activate the cyclic GMP-AMP synthase (cGAS) sensor and trigger inflammatory responses.[12, 13] mtDNA has been shown to bind to various mitochondrial proteins to form nucleoids. The transcription and replication of mtDNA within these nucleoids involves a sophisticated interplay of various proteins.[14, 15] Reducing the release of mtDNA in RTECs was recently shown to provide effective protection against I/R injury as well as cisplatin-induced AKI, highlighting mtDNA as a potential therapeutic target..[16] However, the mechanisms upstream of mtDNA-mediated inflammation in AKI RTECs require further elucidation.

Uracil-DNA glycosylase 1 (UNG1), localized to the mitochondrial matrix and encoded by a gene on human chromosome 12, prevents mtDNA mutations by maintaining the accuracy of mtDNA replication and transcription.[17] It serves as a crucial mitochondrial DNA repair protein in the body. Base excision repair (BER) is a predominant DNA repair pathway in mitochondria, primarily addressing nucleobase lesions and single-strand breaks (SSBs).[18, 19] As a mitochondrial BER enzyme, UNG1 can protect mtDNA from oxidative stress in cells.[20] Recently, Mertz et al. found that UNG1 reduces uracil mutations caused by cytidine deaminase APOBEC3B-induced cytidine deamination during DNA replication, thereby slowing breast cancer development.[21] In addition, blocking UNG1-dependent repair of damaged mtDNA has been shown to lead to mtDNA leakage into the cytoplasm of cells, resulting in testicular injury.[22] Together, these findings suggest that UNG1 plays a crucial protective role in some diseases. However, the role of UNG1 in mtDNA maintenance and AKI inflammatory progression remain unclear. In this study, we validated the protective effects of UNG1 on renal function, mitochondrial structure, and inflammation *in vivo*. We further investigated the impact of UNG1 on mtDNA leakage-mediated inflammation in RTECs and its role in protecting mtDNA. Our aim was to elucidate the mechanisms underlying the inflammatory response in RTECs and identify novel therapeutic targets for AKI.

Results

Mitochondrial dysfunction promotes cGAS-STING-mediated inflammation *in vitro* and *in vivo* during AKI

Mitochondrial damage is found in many types of AKI, and leads to mtDNA breakage and cytosolic release that drives mitochondrial dysfunction-associated inflammation.[24–26] As a DNA sensor, cGAS can recognize and bind to mtDNA fragments, then activate stimulator of interferon genes (STING), which further activates classical NF-kB inflammatory responses.[27, 28] First, we generated an I/R-induced AKI model in C57BL/6J mice. Significant increases in Scr and BUN levels, as well as pathological changes in the kidneys (measured by H&E and PAS staining) confirmed that we had successfully established a model of AKI (Supplementary Fig. 1A-B). Meanwhile, IHC staining revealed that I/R treatment resulted in a marked upregulation in KIM-1 expression levels (Fig. 1A). Moreover, we observed increased

mitochondrial swelling, fragmentation and the breakdown or loss of cristae in I/R-induced AKI mouse kidney samples (Fig. 1B). Next, we established an H/R-induced model of AKI in HK-2 cells and observed a similar increase in KIM-1 mRNA expression levels (Fig. 1C). A significant decrease in ATP levels and SOD activity (Fig. 1D-E), together with an increase in MDA content and ROS levels was found in H/R cells, suggesting that mitochondrial dysfunction had occurred (Fig. 3F-G). Next, we examined mitochondrial morphological changes with Mito-Tracker staining and quantified mitochondrial network parameters. A reduction in mitochondrial networks was observed in AKI cells compared to CON cells, as well as an increase in individual mitochondria, suggesting that AKI induced mitochondrial fragmentation (Fig. 1H). At the same time, a decrease in the mitochondrial membrane potential as measured by JC-1 staining was also observed in H/R-treated cells (Fig. 1I). Finally, transmission electron microscopy images revealed obvious defects in the mitochondrial structures of H/R-treated cells (Fig. 1J). These findings suggest that mitochondrial dysfunction occurs in both *in vivo* and *in vitro* models of AKI.

To investigate the effects of mitochondrial dysfunction on mtDNA in AKI, we measured DNA copy numbers in the mitochondria and cytoplasm of CON and H/R-treated cells. We observed mtDNA leakage into the cytoplasm of H/R-treated cells (Fig. 1K). Since cGAS serves as a cytoplasmic dsDNA sensor that activates STING and triggers inflammation,[29] we next examined mRNA and protein expression levels of components of the cGAS-STING signaling pathway. We found marked activation of the cGAS-STING pathway (Fig. 1L-M), as well as upregulation of the inflammatory cytokines IL-1 and IL-6 in H/R-treated HK-2 cells (Fig. 1N-O). These findings further validate activation of the cGAS-STING pathway-mediated inflammatory response in AKI.

As a key factor in the cGAS-STING pathway, activation of STING during AKI can prompt an inflammatory response.[30] Thus, we next established an I/R-AKI mouse model in *Sting*$^{-/-}$ mice to confirm the role of STING in AKI(Fig. 1P). The knockout efficiency of *Sting* was verified by genotype identification and no pathological changes were observed in the heart, liver, spleen, lung, or kidney (Supplementary Fig. 2A-B). Deletion of STING significantly ameliorated I/R-induced renal dysfunction as measured by changes in Scr and BUN levels (Fig. 1Q). Furthermore, H&E and PAS staining also revealed a marked reduction in tubular injury in *Sting*$^{-/-}$ I/R-AKI mice, including brush border loss, inflammatory cell infiltration, and cast formation (Fig. 1R). Concurrently, IL-1 and IL-6 levels were found to be significantly lower in *Sting*$^{-/-}$ I/R-AKI mice compared to WT I/R-AKI mice (Fig. 1S-T). These findings collectively show that during AKI, mitochondrial dysfunction and increased ROS production lead to mtDNA fragmentation and leakage into the cytoplasm, followed by activation of the cGAS-STING signaling pathway and triggering an inflammatory response. Deletion of STING *in vivo* alleviates renal dysfunction and inflammation. However, the cGAS–STING pathway is regulated by various pathways, and the role of mitochondria during this process is poorly understood.[31]

The mitochondrial protein UNG1 is downregulated in AKI

To investigate the mechanisms of mtDNA-related inflammation during AKI, we analyzed single-cell sequencing data from the kidneys of AKI patients and controls (GSE210622). We identified 58,807 cells

and 15 distinct cell clusters (Fig. 2A). The validity of our cell type classification was confirmed by the expression patterns of established cell type-specific markers (Fig. 2B). Specifically, we found a significant reduction in proximal tubule cells within the AKI group (Fig. 2C). The proximal tubule cell population was annotated into S1S2, S3, circulating, redifferentiating, poorly repaired, and severely damaged subclusters (Fig. 2D-E).[32] As the S1S2 segment of the proximal tubule is highly susceptible to damage during I/R,[33] we focused on the PT_S1S2 subcluster (Fig. 2F) and found that 4571 genes were downregulated in this subcluster. Concurrently, RNA sequencing was performed on H/R-induced HK2 cells to identify genes associated with AKI. A total of 1,676 DEGs were found, as shown in the differential gene heatmap in Fig. 2G. GO analysis of PT_S1S2-specific DEGs and HK-2 DEGs revealed enrichment of multiple mitochondrial-related terms in cellular components, with the “mitochondrion” term containing the largest number of genes (Fig. 2H). To identify genes related to mtDNA-mediated inflammation, we intersected mtDNA-related genes from the Mito-Carta 3.0 database with genes under the “mitochondrion” category from the PT_S1S2 and AKI cell groups. UNG1 was found to be differentially expressed (Fig. 2I). UNG1 localizes to the mitochondria and is a member of the uracil glycosyltransferase family. Studies have shown that UNG1 maintains genomic stability by initiating the BER pathway.[34] Here, we found that UNG1 mRNA and protein expression levels were decreased during AKI (Fig. 2J-K). Similarly, immunofluorescence staining of UNG1 in mouse kidney tissue revealed a significant reduction in UNG1 expression levels in I/R-induced AKI tubular cells (Fig. 2L). In summary, our findings show that UNG1 expression levels are markedly decreased in both AKI patients and RTECs. However, the role and mechanisms of UNG1 in AKI require further investigation.

UNG1 mitigates the mtDNA-related cGAS-STING inflammatory response in H/R-induced AKI

To verify the mtDNA-mediated inflammatory response in AKI, we next detected mtDNA copy numbers in both mitochondrial and cytoplasmic fractions after knockdown and overexpression UNG1 in HK-2 cells (Supplementary Fig. 3A-B). We found that overexpression of UNG1 led to a reduction in mtDNA leakage in AKI cells (Fig. 3A). Overexpression of UNG1 was also found to increase the expression of the mitochondrially-encoded proteins NADH:ubiquinone oxidoreductase core subunit 1 (ND1), cytochrome B (Cyt-B) and cytochrome C oxidase 2 (mtCO2) in AKI cells (Fig. 3B). We further showed that UNG1 overexpression led to a reduction in H/R-induced activation of the cGAS-STING pathway (Fig. 3C). Our IL-1 and IL-6 data also pointed to a protective role for UNG1 in H/R cells (Fig. 3D-E). Together, our results suggest that UNG1 mitigates mtDNA-related inflammatory responses in AKI cells by preventing the leakage of mtDNA into the cytoplasm.

UNG1 protects kidney function in both I/R- and cisplatin-induced AKI mice

Next, we overexpressed UNG1 *in vivo* using the Adeasy adenovirus system to transport the shuttle plasmid pAdEasy-m-*Ung1*-3flag-CMV-Luc (Ad-UNG1) to the mouse kidney, Ad-vector was used as the control and no pathological changes were observed in the heart, liver, spleen, lung, or kidney (Supplementary Fig. 4). Ad-Vector or Ad-UNG1 were injected into the tail veins of mice, then models of AKI were established through bilateral renal artery clamping, as well as intraperitoneal cisplatin

administration (Fig. 4A). Immunofluorescence staining confirmed that UNG1 was successfully overexpressed in mouse kidney tissue (Fig. 4B). Subsequent detection of Scr and BUN levels revealed that UNG1 significantly mitigated the decline in renal function caused by I/R and cisplatin (Fig. 4C-D). H&E and PAS staining revealed that I/R- and cisplatin-induced pathological changes in the renal tubules were mitigated following renal overexpression of UNG1. In addition, overexpression of UNG1 led to a reduction in tubular KIM-1 expression in I/R- and cisplatin-induced AKI (Fig. 4E-F). Transmission electron microscopy images of the mitochondrial structure in the kidneys indicated that the I/R- and cisplatin-induced mitochondrial swelling, loss of cristae, and vacuolation was mitigated by UNG1 (Fig. 4G-H). Next, we investigated the effects of UNG1 overexpression on the cGAS-STING pathway in AKI mouse kidneys and found that UNG1 significantly suppressed activation of the cGAS-STING pathway in I/R- and cisplatin-induced AKI mice (Fig. 4I-J). In addition, our IL-1 and IL-6 data indicated that inflammation was markedly reduced in UNG1-overexpressing AKI mice (Fig. 4K-N). Together, our findings suggest that UNG1 exerts renoprotective effects in I/R- and cisplatin-induced AKI.

UNG1-mediated SSBP1 oligomerization stabilizes mitochondrial nucleoids

UNG1 is a crucial BER enzyme responsible for maintaining mtDNA stability. Mitochondrial BER enzymes have been implicated in regulating the mtDNA-mediated immune response and inflammation.[17] To investigate the protective mechanism of UNG1 during AKI, we extracted proteins from human RTECs and carried out IP studies to identify proteins potentially interacting with UNG1. Silver staining revealed an enriched band for UNG1 (Fig. 5A). Subsequently, we intersected 283 IP-specific proteins with mitochondrial proteins from the Mito-Cata 3.0 database and identified 53 mitochondrial-associated proteins with potential binding to UNG1(Supplementary table.3). Among these 53 proteins, the nucleoid-associated protein SSBP1 was identified as a potential binding partner of UNG1 (Fig. 5B). SSBP1 functions as an important protein associated with the assembly of nucleoids. Specifically, SSBP1 dimers or tetramers bind to ssDNA to prevent the generation of secondary structures of DNA that could impede downstream replication or repair processes.[35] Nucleoid instability is a well-documented cause of mtDNA release from the mitochondria into the cytoplasm. [36] Next, we employed the HDOCK program to perform molecular docking simulations and molecular dynamics simulations on UNG1 and SSBP1 to predict the protein-protein interaction model and potential binding sites between UNG1 and SSBP1. Our analysis revealed that glutamic acid residue 47 on the SSBP1 protein molecule may play a crucial role (Fig. 5C). Subsequently, we validated the interaction between UNG1 and SSBP1 through IP and western blot analyses (Fig. 5D).

Next, we examined whether UNG1 regulates mtDNA stability by affecting SSBP1 levels using UNG1 knockdown. We found that knockdown of UNG1 in normal cells did not affect SSBP1 protein expression levels. However, overexpression of UNG1 under H/R conditions increased SSBP1 protein levels (Fig. 5E). Since SSBP1 functions through oligomerization, we then examined its dimer/tetramer formation and found that SSBP1 oligomer formation was reduced under H/R conditions, while overexpression of UNG1 under H/R conditions enhanced SSBP1 oligomer content. Our findings suggest that UNG1 may influence mitochondrial nucleoid formation by promoting SSBP1 oligomer assembly (Fig. 5F). Similarly, our

immunofluorescence colocalization data revealed that overexpression of UNG1 promoted SSBP1-mtDNA complex formation in H/R cells (Fig. 5G). ChIP studies further demonstrated that UNG1 knockdown reduces the binding of SSBP1 to mtDNA (Fig. 5H). To identify the UNG1-SSBP1 binding site, we mutated glutamic acid at position 47 to the hydrophobic amino acid alanine based on molecular dynamics simulations as mentioned earlier. We first confirmed expression of mutant-SSBP1 in HK-2 cells by IP and western blot analyses (Fig. 5I) and subsequently verified the reduced binding capacity of mutant-SSBP1 to UNG1 (Fig. 5J). Accordingly, protein oligomerization assays revealed reduced oligomer formation in cells overexpressing mutant-SSBP1 (Fig. 5K), while ChIP analysis showed decreased binding between mutant-SSBP1 and mtDNA (Fig. 5L). These findings collectively demonstrate that UNG1 maintains mtDNA stability by promoting formation of the SSBP1-mtDNA complex.

UNG1 attenuates renal inflammation in *Sting*$^{-/-}$ mice with AKI

The STING pathway plays a crucial role in immune responses and has emerged as a compelling target in clinical therapy. Despite promising preclinical studies, clinical trials of STING-targeted drugs have largely failed to deliver durable efficacy.[37] Therefore, investigating the detailed upstream mechanisms of STING may help to unlock the full therapeutic potential of this inflammatory pathway. As previously shown, knockdown of STING has a protective effect *in vivo*. Thus, we generated UNG1-overexpressing *Sting*$^{-/-}$ AKI mice to investigate the relationship between UNG1 and STING deletion in the mtDNA-cGAS-STING inflammatory response. Scr and BUN analyses revealed that overexpression of UNG1 further improves renal function in I/R-induced *Sting*$^{-/-}$ mice (Fig. 6A). H&E and PAS staining showed a significant mitigation of tubular damage in UNG1-overexpressing *Sting*$^{-/-}$ AKI mice and KIM-1 expression also verified that UNG1 plays a protective role (Fig. 6B). Subsequently, we examined the protein expression levels of components of the STING pathway in mouse kidney tissue and found that UNG1 further ameliorated the STING-mediated inflammatory pathway (Fig. 6C). These protective effects were further confirmed in our H/R-induced AKI cellular model following treatment with the STING inhibitor C-176 (Fig. 6D). Moreover, analysis of IL-1 and IL-6 levels revealed that UNG1 reduced inflammatory cytokines *in vivo* and *in vitro* when STING was either knocked out or inhibited (Fig. 6E-H).

Discussion

Mitochondrial dysfunction plays a significant role in the progression of AKI; however, to date, few studies have examined mtDNA-related inflammation and the maintenance of mitochondrial nucleoids in AKI. Here, we focus on the mtDNA-associated protein UNG1, investigating and identifying its role in maintaining mtDNA stability. We show that UNG1 markedly ameliorates renal injury and mitochondrial dysfunction, thus mitigating mtDNA-related inflammation *in vitro* and *in vivo*. Mechanistically, UNG1 promotes SSBP1 oligomer formation, enhancing its binding to damaged mtDNA and maintaining stability of the mtDNA genome. Formation of the SSBP1-mtDNA complex improves mitochondrial function by suppressing mtDNA leakage into the cytoplasm and subsequent activation of the cGAS-STING inflammatory pathway, thereby hindering AKI progression(Fig. 7). Overexpression of UNG1 in the

mitochondria exerts renoprotective effects in *Sting*$^{-/-}$ mice with AKI. Collectively, our findings show that UNG1 may be a promising target for the treatment of AKI.

Numerous studies have reported that mitochondrial dysfunction and inflammation contribute to AKI progression.[38, 39] Mitochondrial damage leads to mtDNA breakage and triggers the cGAS-STING inflammatory response.[40] Thus, targeting the mtDNA-cGAS-STING pathway has the potential to improve AKI. Here, we confirmed that mitochondrial damage and activation of the inflammatory response occur in our I/R-induced mouse and H/R-treated cellular models of AKI. We observed mitochondrial damage in the kidneys of mice with AKI, and mitochondrial dysfunction in H/R-treated HK-2 cells as measured by increased MDA and ROS content, decreased SOD activity, reduced ATP levels, decreased mitochondrial membrane potential, and mitochondrial structural damage. When cGAS detects cytoplasmic DNA, the second messenger cGAMP is produced and binds to STING, thereby triggering STING oligomerization, and promoting its translocation.[41] Recent studies have shown that STING is closely linked to the onset and progression of various diseases.[42–44] To clarify the role of STING in the inflammatory response associated with AKI, we generated *Sting*$^{-/-}$ mice to examine the protective effects of STING deletion on kidney injury. We found that deletion of STING led to a reduction in Scr and BUN levels and improved I/R-induced pathological changes. These findings indicate that STING deletion significantly improves kidney function and reduces kidney inflammation. However, previous studies have shown that STING knockout does not completely eliminate mitochondrial damage or inflammatory responses in AKI mice, suggesting that upstream mitochondrial dysfunction may also participate in AKI progression.[45] Therefore, we next sought to identify potential targets upstream of the cGAS-STING pathway. Through RNA sequencing analysis, we identified UNG1 as a downregulated mtDNA-related gene in both AKI patients and RTECs and validated its expression *in vitro* and *in vivo*. Several studies have reported that UNG is associated with the progression of diverse diseases and may be a potential target for therapeutic intervention.[46–48] However, the mitochondrial isoform UNG1 and its role in acute kidney diseases are poorly understood. Inhibition of UNG enzyme activity in the nucleus has previously been shown to lead to a reduction in APOBEC3-associated mutations and other overall clustered mutations in human breast cancer cells, suggesting that UNG may be a potential therapeutic target.[49] Furthermore, UNG functions as an important BER enzyme that eliminates uracil bases to reduce base mismatches.[50] Thus, we next examined mtDNA copy numbers in HK-2 cells and found that UNG1 reduced mtDNA leakage and mitigated the cGAS-STING inflammatory pathway. These findings suggest that UNG1 exerts a crucial protective role in reducing tubular epithelial cell inflammation during AKI. To evaluate its nephroprotective effects, we further overexpressed UNG1 in mouse kidneys and established I/R- and cisplatin-induced AKI models. We found that UNG1 significantly restored renal function, reduced tubular pathological changes and decreased KIM-1 expression in AKI mice. Consistently, UNG1 markedly mitigated mitochondrial structural damage and reduced activation of the cGAS-STING pathway in mouse kidneys. Thus, our findings suggest that UNG1 exerts a protective effect on the kidneys of AKI mice.

Recent studies have confirmed that mtDNA forms nucleoids by tightly associating with multiple proteins, which ensure the maintenance, replication, and translation of mtDNA.[51] The formation of mitochondrial

nucleoids is closely linked to mtDNA homeostasis.[52] mtDNA homeostasis is regulated by a variety of factors and involved in the progression of various diseases.[53–56] Previous studies have reported that overexpression of UNG1 protects mtDNA from oxidation.[20] However, the role of UNG1 in mtDNA repair remains poorly characterized. Therefore, we used mass spectrometry and databases to identify molecules with potential binding affinity to UNG1 and identified SSBP1, a key component of nucleoids. Co-IP further confirmed specific binding between UNG1 and SSBP1. The mitochondrial nucleoid is a complex assembly primarily composed of mtDNA and various proteins involved in transcription and replication, including SSBP1.[57] Recent studies have found that SSBP1 depletion in the mitochondria results in mitochondrial dysfunction in lung adenocarcinoma.[58] Here, we found that overexpression of UNG1 significantly increases SSBP1 expression levels under H/R conditions, but has no effect on SSBP1 protein expression levels under normal conditions. Interestingly, SSBP1 mutations reportedly reduce oligomer formation, thus impairing nucleoid and mtDNA replication, and subsequently affecting replisome machinery in optic atrophy disorder.[59] Using an oligomerization assay, we confirmed that UNG1 promotes SSBP1 dimer/tetramer formation during AKI. Immunofluorescence staining revealed co-localization among mtDNA, mitochondria, and SSBP1. ChIP experiments further verified that UNG1 knockdown significantly impaired SSBP1 binding to mtDNA. We also generated SSBP1 mutants and found that SSBP1 mutations reduced SSBP1 oligomer formation and SSBP1-mtDNA binding. These findings indicate that UNG1 regulates SSBP1 dimer/tetramer formation, promotes SSBP1-mtDNA nucleoid assembly, reduces mtDNA damage and leakage, and consequently alleviates tubular epithelial cell inflammation.

STING is a potential therapeutic target for cancer. However, several barriers to the use of STING-targeted immunotherapy remain, including drug delivery, molecular design, and combination strategies.[60–62] Current research has confirmed that stress-induced mtDNA leakage is a key driver of STING activation.[63] Meanwhile, genetic deletion, pharmacological suppression of STING, and blockage of mtDNA release have been shown to significantly decrease inflammatory reactions.[64] However, the relationship between mtDNA homeostasis and STING in kidney disease remains unclear. Here, we investigated the nephroprotective effects of mtDNA-related protein UNG1 in *Sting*$^{-/-}$ mice by overexpressing UNG1 in *Sting*$^{-/-}$ AKI mice. We found that UNG1 overexpression further alleviates renal dysfunction and pathological changes in the renal tubules of *Sting*$^{-/-}$ mice. KIM-1 expression was also significantly reduced in UNG1-overexpressing *Sting*$^{-/-}$ AKI mice. In addition, previous studies have highlighted the significance of inhibiting STING-related inflammation in alleviating kidney injury.[65] We found that UNG1 suppressed the STING-induced inflammatory response; knockdown of STING led to decreased expression of downstream molecules and a reduction in IL-1 and IL-6 levels. Together, our findings show that UNG1 can improve renal dysfunction, ameliorate pathological damage, and resolve inflammation, and strongly suggest that UNG1 is a potential therapeutic target in AKI.

In summary, the mtDNA-related gene UNG1 is downregulated in the RTECs of AKI patients. We show that UNG1 alleviates mitochondrial dysfunction and mtDNA-mediated inflammatory responses *in vitro* and *in*

vivo. UNG1 maintains mtDNA stability by binding to SSBP1 and promoting SSBP1-mtDNA complex formation, thus reducing mtDNA-cGAS-STING inflammatory responses. Our findings provide robust scientific evidence supporting UNG1 as a potential therapeutic target for AKI.

Materials and Methods

Animals and mice models

Male C57BL/6J mice weighing 20–24 g were purchased from Chongqing Medical University Animal Center (Chongqing, China). Mice were housed in specific pathogen-free (SPF) conditions at 22 ± 2°C, 50–60% humidity and with a 12/12 h light/dark cycle. All animal procedures were performed in accordance with the guidelines outlined by the China Council on Animal Care and Use and were approved by the Institutional Animal Ethical Committee of Chongqing Medical University (IACUC-CQMU-2024-10117). To establish I/R-induced AKI model, mice were anesthetized with tribromoethanol (Dowobio, Shanghai, China) and placed in a supine position. Bilateral renal pedicles were separated carefully and clamped with nontraumatic vascular clips for 25 min. As a control, sham mice underwent the identical procedure without clamping the renal pedicles. All surgical groups of mice were humanely killed 24 h after reperfusion. For cisplatin-induced AKI, mice were intraperitoneally injected with 20 mg/kg cisplatin. As a control, littermates were administered an equivalent volume of normal saline.

Overexpression of UNG1 and knockout of *Sting* in AKI mouse model

Ad-Adeasy-m-Ung1-3xflag-LUC (Adv-UNG1, 1.99×10^{11} PFU/mL) and Ad-Adeasy-LUC (Adv-vector, 1.58×10^{11} PFU/mL) purchased from HanBio (Shanghai, China), were administered via tail vein injection into AKI and control mice, respectively. Male C57BL/6J mice were randomly assigned to the following six groups (n = 6 mice per group): sham, I/R, saline, cisplatin, I/R+UNG1, and cisplatin+UNG1.

Sting-knockout (*Sting*$^{-/-}$, C57BL/6J background) mice were obtained from Cyagen (Suzhou, China). Genotyping was performed by polymerase chain reaction (PCR) using genomic DNA extracted from tail tissue of mice aged 2–3 weeks. The following PCR primers were used to genotype the *Sting*$^{-/-}$ mice: F1: 5'-ACCTGGTTTATGGAGGCTGGTAG-3'; and R1: 5'-AATGTTCCTTCTCCCTCTCGCC-3'. The PCR primers used for wild-type (WT) mice were: F1: 5'-ACCTGGTTTATGGAGGCTGGTAG-3'; and R2: 5'-TGGGCTACTCTTGGATACACCTC-3'. The PCR product band was 495 base pairs for the mutant (*Sting*$^{-/-}$) mice, and 515 base pairs for the WT mice. WT and *Sting*$^{-/-}$ mice were further randomized into five groups: sham, *Sting*$^{-/-}$, I/R, *Sting*$^{-/-}$+I/R, and *Sting*$^{-/-}$+I/R+UNG1.

Cell culture

The human renal tubular epithelial cell line HK-2 was purchased from Procell Life Science & Technology (Wuhan, China) and cultured in DMEM/F12 complete medium (HyCyte, China) at 37°C and 5% CO_2 with normal oxygen. Hypoxia/reoxygenation (H/R) treatment was used to generate a cellular model of AKI.

Briefly, cells were cultured for 12 h in glucose-free DMEM (Gibco, US) in a tri-gas incubator with a N_2 concentration of 94%, CO_2 concentration of 5% and O_2 concentration of 1%, then cultured under normal culture conditions for 24 h.

Gene silencing or overexpression

HK-2 cells were cultured in 6-well plates and transiently transfected with siRNA or plasmid (Tsingke Biotechnology Co., Ltd., China). The sense sequence for si-UNG1 was 5'-GGCUCUGCUUUAGUGUUCA-3', while a non-silencing siRNA oligonucleotide that did not recognize any known homolog of mammalian genes was employed as the negative control. The UNG1-overexpressing plasmid was confirmed by DNA sequencing, with the empty pcDNA3.1 vector serving as the corresponding control. negative control. siRNA and plasmid transfections were performed out using Lipofectamine 2000 reagent (11668030, Thermo Fisher Scientific, USA), in accordance with the manufacturer's protocol. he efficiency of target gene knockdown or overexpression was validated by quantitative real-time polymerase chain reaction (qPCR).

Biochemical assay

Serum creatine (Scr) and blood urea nitrogen (BUN) concentrations were detected in the serum using commercial assay kits (Nanjing Jiancheng, Nanjing, China), according to the manufacturer's protocol.

Histology and immunohistochemical (IHC) staining

Formalin-fixed kidney tissue samples were embedded in paraffin and sectioned into slices (4 μm thick). The tissue sections were then stained with hematoxylin and eosin (H&E) and periodic acid-Schiff (PAS) to assess renal histopathological changes. The degree of renal interstitial damage was scored from 0 to 5. For IHC staining, antigen retrieval was performed by heating samples for 10 min at 98^{o}C with Tris-EDTA buffer pH 9.0. Samples were stained using an antibody against kidney injury molecule-1 (KIM-1) (1:200, ab323414, Abcam, UK). Sections were visualized by microscopy, and the positive intensities of KIM-1 were evaluated using ImageJ software (NIH, USA).

Transmission electron microscopy

Mitochondrial ultrastructure was examined by standard transmission electron microscopy. Fresh renal tissues were fixed overnight in a solution containing 2% paraformaldehyde and 2.5% glutaraldehyde, then washed, dehydrated, and embedded in resin following to standard procedures. The embedded specimens were analyzed using a HT7800/HT7700 transmission electron microscope.

RNA extraction and qPCR

Total RNA was isolated with the SteadyPure Quick RNA Extraction Kit (Accurate Biology, China). For mRNA quantification, cDNA was synthesized using the PrimeScript RT Reagent Kit (Takara, Japan), and qPCR was carried out with TB Green Premix Ex Taq (Takara, Japan). Relative mRNA expression was

analyzed by the $2^{-\triangle\triangle Ct}$ method, normalized to GAPDH. The primer sequences used in this study are listed in Table S1.

Measurement of ATP levels

The concentration of ATP in HK-2 cells was quantified using an Enhanced ATP Assay Kit (Beyotime Biotechnology, China), following the manufacturer's protocol.

Measurement of mitochondrial reactive oxygen species (ROS)

ROS levels were evaluated in HK-2 cells using the ROS Assay Kit (Beyotime Biotechnology, China). Briefly, cells were incubated with DCFH-DA for 30 min in the dark at 37^{o}C. After washing, cells were analyzed by flow cytometry.

DNA isolation and mtDNA copy number assay

HK-2 cells were separated into two equal-volume aliquots, one for whole-cell DNA extraction using the DNeasy Blood & Tissue Kit (Qiagen, Germany), and the other for mitochondrial and cytoplasmic isolation using the Cell Mitochondria Isolation Kit (Beyotime Biotechnology, China), following the respective manufacturer's protocol. DNA was then extracted from the mitochondrial and cytosolic fractions using the DNeasy Blood & Tissue Kit (Qiagen, Germany). qPCR was conducted on whole-cell lysates, mitochondria and cytosolic fractions using mtDNA-specific primers, yielding cycle threshold (CT) values that indicated mtDNA abundance.

Western blot

Kidney tissues and cells were lysed with RIPA buffer. The total protein concentration was quantified using the BCA Protein Assay Kit (Beyotime Biotechnology, China). Equivalent amounts of protein were separated by 7.5–12% SDS-PAGE and transferred onto PVDF membranes, which were blocked and incubated overnight with specific primary antibodies at 4^{o}C. The following primary antibodies were used: anti-cGAS (1:1000, Cell Signaling Technology, US), anti-STING (1:1000, Cell Signaling Technology, US), anti-TBK1 (1:1000, Cell Signaling Technology, US), anti-p-TBK1 (1:1000, Cell Signaling Technology, US), anti-NF-κB-p65 (1:1000, Cell Signaling Technology, US), anti-p-NF-κB-p65 (1:1000, Cell Signaling Technology, US), anti-UNG1 (1:1000, Abcam, UK), anti-COX IV (1:1000, Proteintech, China), anti-ND1 (1:1000, Proteintech, China), anti-Cyt-B (1:1000, Proteintech, China), anti-mtCO2 (1:1000, Proteintech, China), anti-SSBP1 (1:1000, Proteintech, China) and anti-β-actin (1:2500, Proteintech, China). Subsequently, the membranes were incubated with secondary antibodies (1:5000, Proteintech, China) for 1 h at room temperature. Protein bands were visualized using the ECL immunoblot detection system and band intensities were analyzed using ImageJ software (NIH, USA).

ELISA assays

The concentrations of IL-1β and IL-6 in kidney homogenate and HK-2 cells were quantified using the corresponding commercially available ELISA kits (Jiangsu Meimian Industrial Co., Ltd, China) according to the manufacturer's instructions.

Immunofluorescence staining

Tissue sections were incubated with primary antibodies overnight, followed by incubation with goat anti-rabbit IgG conjugated with Alexa Fluor 594 (Beyotime Biotechnology, China). Samples were then incubated with lotus tetragonolobus lectin (LTL, Invitrogen, US) as a marker for proximal tubules and the nuclear stain 4,6-diamidino-2-phenylindole (DAPI) for 10 min at room temperature. Sections were visualized using a fluorescence microscope. HK-2 cells were stained using MitoTracker Red FM Dye (Invitrogen, US), then fixed with 4% paraformaldehyde for 30 min and permeabilized with 0.5% Triton X-100 for 10 min. Samples were blocked with 1% bovine serum albumin for 1 h at room temperature, incubated with primary antibodies overnight, followed by incubation with goat anti-rabbit IgG conjugated with Alexa Fluor 594 or 488 (1:200, Beyotime Biotechnology, China) for 1 h at 37^{O}C. Nuclei were stained with DAPI for 10 min at room temperature. The primary antibodies used in this study were as follows: anti-dsDNA (1:1000, Abcam, UK), and anti-SSBP1 (1:50, Proteintech, China). Images were captured by confocal laser scanning biological microscopy (Leica, Germany).

Cellular superoxide dismutase (SOD) and malondialdehyde (MDA) assays

SOD and MDA levels were detected in the lysate of HK-2 cells using commercially available reagents for SOD and MDA (Nanjing Jiancheng, China) according to the manufacturer's instructions.

JC-1 mitochondrial membrane potential assay

The mitochondrial membrane potential of HK-2 cells was detected using the JC-1 fluorescent probe (Beyotime Biotechnology, China), in accordance with the manufacturer's instructions. Briefly, cells were incubated with JC-1 solution for 30 min at 37^{O}C. After washing, cells were visualized and photographed using a fluorescent microscope (Leica, Germany). Fluorescence intensities were analyzed using ImageJ software (NIH, USA).

Co-immunoprecipitation (co-IP) and mass spectrometry

HK-2 cells were lysed with IP lysis buffer containing protease inhibitor cocktails, then the total protein concentration was determined using the BCA Assay Kit. The lysate supernatant was incubated with primary antibody for 12 h at 4^{O}C, then the protein A/G agarose mixture was added to capture the immunocomplexes. Next, the immunocomplexes were washed three times with precooled IP lysis/wash buffer, and analyzed by mass spectrometry. Western blot analysis was also performed on co-IP samples. After boiling in SDS-PAGE loading buffer, samples were separated by SDS-PAGE and incubated with the following primary antibodies: anti-UNG1, anti-SSBP1, anti-FLAG, and anti-IgG .

Molecular docking and molecular dynamics simulation

Molecular docking was used to predict the potential binding between UNG1 and mitochondrial single-stranded DNA binding protein 1 (SSBP1). The structures of UNG1 and SSBP1 were obtained from PubChem (CID: 31553) and the Protein Data Bank (PDB ID: 3AJO), respectively. Molecular docking was performed using the HDOCK program to obtain the initial complex structure. A stable complex structure (100.pdb) was obtained through molecular dynamics simulation. Results were analyzed and visualized using PyMOL software (Version 3.0.3). The protein-protein docking score between SSBP1 and UNG1 proteins was – 261.07. The docking score was calculated using the knowledge-based iterative scoring functions ITScorePP or ITScorePR. Molecular dynamics simulations were performed using the GROMACS 2023.4 program.

Generation of the mutant-SSBP1 plasmid

We generated a FLAG-tagged plasmid containing mutant SSBP1 with a glutamic acid to alanine mutation at position 47. The mutation was confirmed by DNA sequencing. A pcDNA3.1 plasmid carrying FLAG-tagged WT-SSBP1 was used as the control. Cells were transfected with the plasmids using Lipofectamine 2000 reagent (Thermo Fisher Scientific, 11668030), according to the manufacturer's protocol. IP and western blotting were performed to confirm the expression of WT and mutant SSBP1.

Oligomerization assay

SSBP1 oligomerization was carried out as described previously.[23] Briefly, Protein isolated from HK-2 cells was treated with or without the crosslinking agent (glutaraldehyde (GA)) at a concentration of 0.1%. The reaction was quenched after 10 min with 0.1 mol/L PBS/ glycine. Monomers, dimers or tetramers were detected by SDS-PAGE. Densitometric analysis was carried out using ImageJ software (NIH, USA).

Chromatin immunoprecipitation (ChIP) assay

DNA was cross-linked with 1% formaldehyde for 10 min, and the reaction was stopped using 0.125 mol/L glycine. Cell lysates prepared from digitonin extracts were incubated for 1 h at 4^{o}C with protein A agarose/salmon sperm DNA, which had been pretreated with anti-SSBP1 (Proteintech, China) or normal rabbit IgG (Beyotime Biotechnology, China) antibody for 12h at 4^{o}C. Complexes were obtained by centrifugation and washed five times with co-IP buffer. DNA was isolated from these protein complexes using The SimpleChIP® Enzymatic Chromatin IP Kit (Magnetic Beads) (Cell Signaling Technology, 9003). qPCR was performed using mtDNA primers.

RNA sequencing and informatics analysis

Total RNA was isolated from normal and H/R-treated HK-2 cells using TRIzol Reagent (Invitrogen, China) according to the manufacturer's instructions. RNA quality, purity, and quantity were assessed by Wuhan Metware Metabolic Biotechnology Co., Ltd. High-throughput RNA sequencing was performed on an Illumina HiSeq x Ten Sequencing System. Differentially expressed genes (DEGs) were filtered using the significant threshold value (P value), fold change (FC), and false discovery rate (FDR). Next, pathway

analysis was performed on the DEGs to identify significantly enriched pathways in the Gene Ontology (GO) database. The significance threshold was defined by the P-value and FDR under the following criteria: |FC|>1.8 and FDR < 0.05. The single-cell sequencing data was obtained from GSE210622, the sample information was listed in table. S2

Statistical analysis

Graphing and statistical analyses were performed using GraphPad Prism 9. Experimental data were expressed as the mean ± SD. Statistical significance between groups was determined using a two-tailed t-test or one-way ANOVA followed by LSD or Dunnett *post hoc* test. P-values of < 0.05 were considered significant.

Declarations

Funding

This work was supported by the National Natural Science Foundation of China (82570849), CQMU Program for Youth Innovation in Future Medicine (W0173), Scientific and Technological Plan Program of Nanchuan District, Chongqing (Cx202327), China Postdoctoral Science Foundation(2025MD774164), Natural Science Foundation of Chongqing (CSTB2025NSCQ-GPX1233).

Competing Interests

The authors have declared that no competing interest exists.

Ethics approval

All animal procedures were performed in accordance with the guidelines outlined by the China Council on Animal Care and Use and were approved by the Institutional Animal Ethical Committee of Chongqing Medical University (IACUC-CQMU-2024-10117).

Legends

Author contributions

CX.W. Writing–original draft, Investigation, Data analysis, Methodology, Funding acquisition. W.T. Investigation, Methodology, Data analysis. P.X: Methodology, Investigation, Writing – review & editing. YT.W. Resources, Methodology. S.H: Writing – review & editing, Data curation, Funding acquisition. PF. Y. Resources, Conceptualization. GQ.Y. Methodology, Investigation. Z.Z: Supervision, Funding acquisition, Conceptualization. XH. L. Writing – review & editing, Supervision, Resources, Funding acquisition, Conceptualization.

Data availability

All data generated are presented in the manuscript or supplementary files. Publicly available datasets analyzed were sourced from Mouse MitoCarta3.0 (https://www.broadinstitute.org/mitocarta/mitocarta30-inventory-mammalian-mitochondrial-proteins-and-pathways), GEO database (https://www.ncbi.nlm.nih.gov/geo/query/acc.cgi?acc=GSE210622).

References

1. Kellum, J.A., et al., *Acute kidney injury*. Nature Reviews Disease Primers, 2021. 7(1).
2. Ostermann, M., et al., *Acute kidney injury*. The Lancet, 2025. 405(10474).
3. Hoste, E.A.J., et al., *Global epidemiology and outcomes of acute kidney injury*. Nature Reviews Nephrology, 2018. 14(10).
4. Xu, X., et al., *Acute kidney injury: pathogenesis and therapeutic interventions*. Molecular Biomedicine, 2025. 6(1).
5. Bhargava, P. and R.G. Schnellmann, *Mitochondrial energetics in the kidney*. Nat Rev Nephrol, 2017. 13(10).
6. Gao, P., et al., *Matricellular protein SMOC2 safeguards tubular integrity in acute kidney injury via integrin β3-dependent inhibition of CCND1-CDK4/6 axis*. Molecular Biomedicine, 2026. 7(1).
7. Kumar, S., *Cellular and molecular pathways of renal repair after acute kidney injury*. Kidney International, 2018. 93(1).
8. Jacobs, M.E., et al., *Endothelial to mesenchymal transition in kidney fibrosis*. Nephrology Dialysis Transplantation, 2024. 39(5).
9. Li, B., et al., *Histone H3K27 methyltransferase EZH2 regulates apoptotic and inflammatory responses in sepsis-induced AKI*. Theranostics, 2023. 13(6).
10. Yan, J., et al., *Renal inflammaging: Mechanisms, pathophysiology and therapeutic prospects*. Ageing Research Reviews, 2026. 118.
11. Jauhari, A., et al., *Mitochondrial DNA: a molecular switch driving sterile neuroinflammation*. Translational Neurodegeneration, 2026. 15(1).
12. Bai, J. and F. Liu, *cGAS–STING signaling and function in metabolism and kidney diseases*. J Mol Cell Biol, 2021. 13(10).
13. Chen, J., et al., *Cellular senescence of renal tubular epithelial cells in acute kidney injury*. Cell Death Discovery, 2024. 10(1).
14. Liu, H., H. Zhuang, and D. Feng, *Quality control of mitochondrial nucleoids*. Trends in Cell Biology, 2025.
15. Yang, M., et al., *Mitochondrial transcription factor a as a guardian of mitochondrial integrity and emerging therapeutic target in human diseases: A review*. International Journal of Biological Macromolecules, 2025. 319.

16. Zhang, C., et al., *Renal-tubular-mitochondrial sequentially targeted nanoagent breaks the vicious cycle of oxidative stress and mtDNA-driven inflammation in acute kidney injury therapy*. Journal of Nanobiotechnology, 2026. 24(1).
17. Urrutia, K., et al., *DNA sequence and lesion-dependent mitochondrial transcription factor A (TFAM)-DNA-binding modulates DNA repair activities and products*. Nucleic Acids Research, 2024. 52(22).
18. Szymanski, M.R., et al., *Human EXOG Possesses Strong AP Hydrolysis Activity: Implication on Mitochondrial DNA Base Excision Repair*. Journal of the American Chemical Society, 2022. 144(51).
19. *Enzymology of mitochondrial DNA repair*, in *DNA Repair*. 2019.
20. Liu, Z., et al., *Hydrogen peroxide mediated mitochondrial UNG1-PRDX3 interaction and UNG1 degradation*. Free Radical Biology and Medicine, 2016. 99.
21. Mertz, T.M., et al., *Genetic inhibitors of APOBEC3B-induced mutagenesis*. Genome Research, 2023. 33(9).
22. Ouyang, K.-W., et al., *m6A-methylated Lonp1 drives mitochondrial proteostasis stress to induce testicular pyroptosis upon environmental cadmium exposure*. Science of The Total Environment, 2024. 931.
23. Del Dotto, V., et al., *SSBP1 mutations cause mtDNA depletion underlying a complex optic atrophy disorder*. J Clin Invest, 2020. 130(1).
24. Bhatia, D., A. Capili, and M.E. Choi, *Mitochondrial dysfunction in kidney injury, inflammation, and disease: Potential therapeutic approaches*. Kidney Research and Clinical Practice, 2020. 39(3).
25. Emma, F., et al., *Mitochondrial dysfunction in inherited renal disease and acute kidney injury*. Nature Reviews Nephrology, 2016. 12(5).
26. Sharma, A., et al., *Therapeutic targeting of the mitochondrial dysfunction-PANoptosis axis: Mechanistic insights and emerging strategies*. Translational Research, 2026. 291.
27. Hu, K., et al., *Revisiting osteoarthritis pathogenesis through the lens of cGAS-STING: Mitochondrial damage, pyroptosis, and inflammatory cascades*. Journal of Orthopaedic Translation, 2026. 56.
28. Liu, J., Z. Jia, and W. Gong, *Circulating Mitochondrial DNA Stimulates Innate Immune Signaling Pathways to Mediate Acute Kidney Injury*. Frontiers in Immunology, 2021. 12.
29. Meichsner, A., V. Bader, and K.F. Winklhofer, *Mitochondria as sources and targets of cellular signaling*. Molecular Cell, 2026. 86(3).
30. Wang, Y., et al., *STING signaling pathway: An oasis in the glioblastoma immune desert*. Theranostics, 2026. 16(7).
31. Vasiyani, H., *Chronic and non-canonical cGAS–STING activation: implications for health, disease, cancer, and emerging therapeutic opportunities*. Apoptosis, 2026. 31(2).
32. Wen, Y., et al., *Analysis of the human kidney transcriptome and plasma proteome identifies markers of proximal tubule maladaptation to injury*. Science Translational Medicine, 2023. 15(726).
33. Chen, Z., et al., *Multi-omics analysis identifies S100a10/Anxa2 complex within proximal tubule aggravates acute kidney injury through p-Stat3/Spp1 signaling*. Translational Research, 2025. 284.

34. Sarno, A., et al., *Uracil–DNA glycosylase UNG1 isoform variant supports class switch recombination and repairs nuclear genomic uracil*. Nucleic Acids Research, 2019. 47(9).
35. Riccio, Amanda A., et al., *Structures of the mitochondrial single-stranded DNA binding protein with DNA and DNA polymerase γ*. Nucleic Acids Research, 2024. 52(17).
36. Giordano, L., et al., *Mitochondrial DNA signals driving immune responses: Why, How, Where?* Cell Communication and Signaling, 2025. 23(1).
37. Shi, J., et al., *Precision targeting of STING: Challenges, innovations, and clinical outlook for cancer therapy*. The Innovation, 2026. 7(1).
38. Sharma, R., et al., *Endothelial prolyl hydroxylase 3 mitigates maladaptive inflammation to promote post-ischemic kidney repair*. Kidney International, 2026.
39. Li, Y., et al., *Tubular EZH2 promotes acute kidney injury by Inhibiting SDHC-mediated mitochondrial function*. Free Radical Biology and Medicine, 2026. 248.
40. Gong, Q., et al., *CX3CL1 deficiency ameliorates acute kidney injury by inhibiting macrophage mitochondrial dysfunction and mtDNA-cGAS-STING signaling*. Cell Death Discovery, 2025. 12(1).
41. Srikanth, S., et al., *The Ca2 + sensor STIM1 regulates the type I interferon response by retaining the signaling adaptor STING at the endoplasmic reticulum*. Nature Immunology, 2019. 20(2).
42. Alipour-Khezri, E., et al., *Cytosolic DNA sensing pathway in senescence and aging: Underlying mechanisms and targeted interventions*. Biomedicine & Pharmacotherapy, 2025. 193.
43. Wang, J., et al., *STING Activation in Various Cell Types in Metabolic Dysfunction-Associated Steatotic Liver Disease*. Liver International, 2025. 45(4).
44. Maekawa, H., et al., *Mitochondrial Damage Causes Inflammation via cGAS-STING Signaling in Acute Kidney Injury*. Cell Rep, 2019. 29(5).
45. Wang, L., et al., *The effects of cGAS-STING inhibition in liver disease, kidney disease, and cellular senescence*. Frontiers in Immunology, 2024. 15.
46. Yang, J.-j., et al., *Silencing Uracil-DNA glycosylase inhibits colorectal cancer progression*. Cancer Cell International, 2026. 26(1).
47. Lee, H., et al., *Mitochondrial DNA editing in mice with DddA-TALE fusion deaminases*. Nature Communications, 2021. 12(1).
48. Kato, A., et al., *Herpes simplex virus 1 evades APOBEC1-mediated immunity via its uracil-DNA glycosylase in mice*. Nature Microbiology, 2025. 10(7).
49. Petljak, M., et al., *Mechanisms of APOBEC3 mutagenesis in human cancer cells*. Nature, 2022. 607(7920).
50. Lu, Y., et al., *Coupling photoelectrochemical and electrochemical strategies in one probe electrode: Toward sensitive and reliable dual-signal bioassay for uracil-DNA glycosylase activity*. Biosensors and Bioelectronics, 2019. 142.
51. Fu, T., et al., *Mitochondrial DNA homeostasis: A novel therapeutic target for neurodegenerative diseases*. Neural Regeneration Research, 2025.

52. Kakudji, E.V. and S.C. Lewis, *Mitochondrial nucleoids.* Current Biology, 2024. 34(21).
53. Bhattacharjee, S., et al., *PRMT5 in mitochondria regulates mtDNA stability through TFAM arginine methylation*. Nature Communications, 2026. 17(1).
54. Chen, Q., et al., *Phase separation in mitochondrial fate and mitochondrial diseases.* Proceedings of the National Academy of Sciences, 2025. 122(21).
55. Zhou, Z., et al., *Muscle metabolic resilience and enhanced exercise adaptation by Esr1-induced remodeling of mitochondrial cristae-nucleoid architecture in males*. Cell Reports Medicine, 2025. 6(5).
56. Gómez-Bañuelos, E., et al., *Anti-TFAM antibodies link mitochondrial damage with antiphospholipid syndrome and thrombosis in SLE*. Annals of the Rheumatic Diseases, 2025. 84(9).
57. Macuada, J., I. Molina-Riquelme, and V. Eisner, *How are mitochondrial nucleoids trafficked?* Trends in Cell Biology, 2025. 35(3).
58. Cui, H., et al., *HMGB3 promotes brain metastasis of lung adenocarcinoma by recruiting SSBP1 for nuclear translocation to remodel mitochondrial metabolism*. Cancer Communications, 2025. 45(12).
59. Del Dotto, V., et al., *SSBP1 mutations cause mtDNA depletion underlying a complex optic atrophy disorder*. Journal of Clinical Investigation, 2019. 130(1).
60. Wang, Y., et al., *cGAS-STING pathway in cancer biotherapy*. Molecular Cancer, 2020. 19(1).
61. Malli Cetinbas, N., et al., *Tumor cell-directed STING agonist antibody-drug conjugates induce type III interferons and anti-tumor innate immune responses*. Nature Communications, 2024. 15(1).
62. Melero, I., et al., *Intratumoural administration and tumour tissue targeting of cancer immunotherapies*. Nature Reviews Clinical Oncology, 2021. 18(9).
63. Huang, N., et al., *The roles of the mtDNA-cGAS-STING axis in tumor immunity: from immune activation to immune evasion*. Frontiers in Immunology, 2026. 16.
64. Ouyang, W., et al., *The cGAS-STING pathway-dependent sensing of mitochondrial DNA mediates ocular surface inflammation*. Signal Transduction and Targeted Therapy, 2023. 8(1).
65. Zhou, X., et al., *Discovery of 3,4-dihydroisoquinoline-2(1H)-carboxamide STING inhibitors as anti-inflammatory agents*. European Journal of Medicinal Chemistry, 2025. 297.

Figures

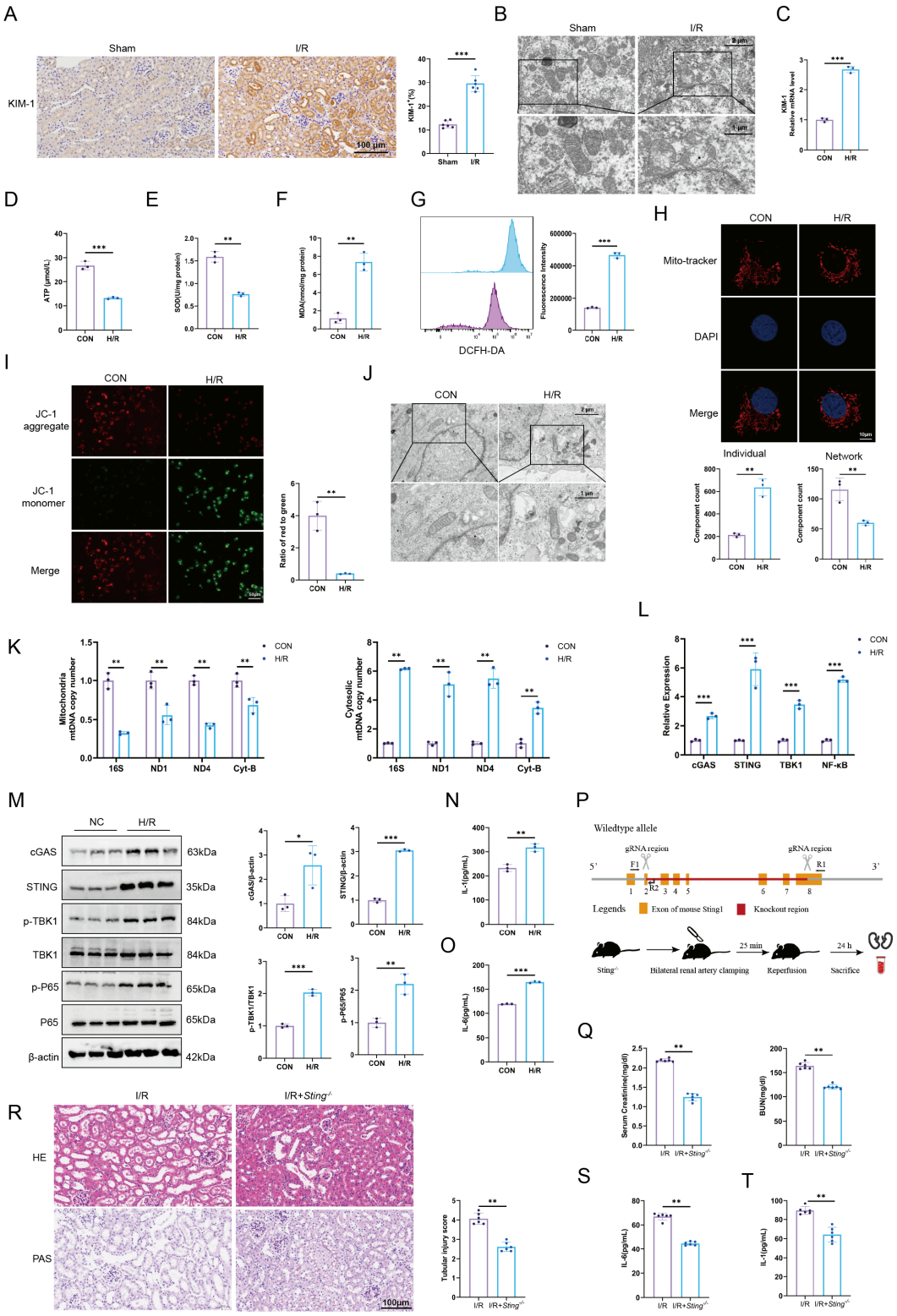


Figure 1

Mitochondrial dysfunction promotes cGAS-STING-mediated inflammation *in vitro* and *in vivo* during AKI. (A) Representative IHC images and quantitative analysis of KIM-1 staining (n = 6, scale bar = 100 μm). (B) Representative TEM images of mouse kidneys (scale bar = 2 μm upper panel, scale bar = 1 μm lower panel). (C) Relative mRNA expression levels of KIM-1 (n = 3). (D-G) ATP, SOD, MDA and ROS levels in HK-2 cells (n = 3). (H) Representative images showing Mito-tracker staining in HK-2 cells (scale bar = 10

μm). MiNa-based quantification of mitochondrial morphological parameters, including individual mitochondria and mitochondrial networks (n = 3). (I) Representative images and quantitative analysis of JC-1 staining in HK-2 cells (scale bar = 50 μm, n = 3). (J) Representative TEM images of HK-2 cells (scale bar = 2 μm upper panel, scale bar = 1 μm lower panel). (K) mtDNA copy number (16S, ND1, ND4 and Cyt-B) in the mitochondria and cytoplasm of HK-2 cells (n = 3). (L) Relative mRNA expression levels of components of the cGAS-STING pathway (n = 3). (M) Western blot analysis and quantification of protein expression levels of components of the cGAS-STING pathway (n = 3). (N-O) IL-1 and IL-6 levels were detected in HK-2 cells by ELISA (n = 3). (P) Schematic diagram showing the generation of *Sting*$^{-/-}$ knockout mice and experimental design. (Q) Scr and BUN levels (n = 6). (R) H&E and PAS staining of kidney sections, and the tubular injury score (n = 6, scale bar = 100 μm). (S-T) IL-1 and IL-6 levels were detected in the kidneys of *Sting*$^{-/-}$ mice by ELISA (n = 6). **P* < 0.05, ***P* < 0.01, ****P* < 0.001.

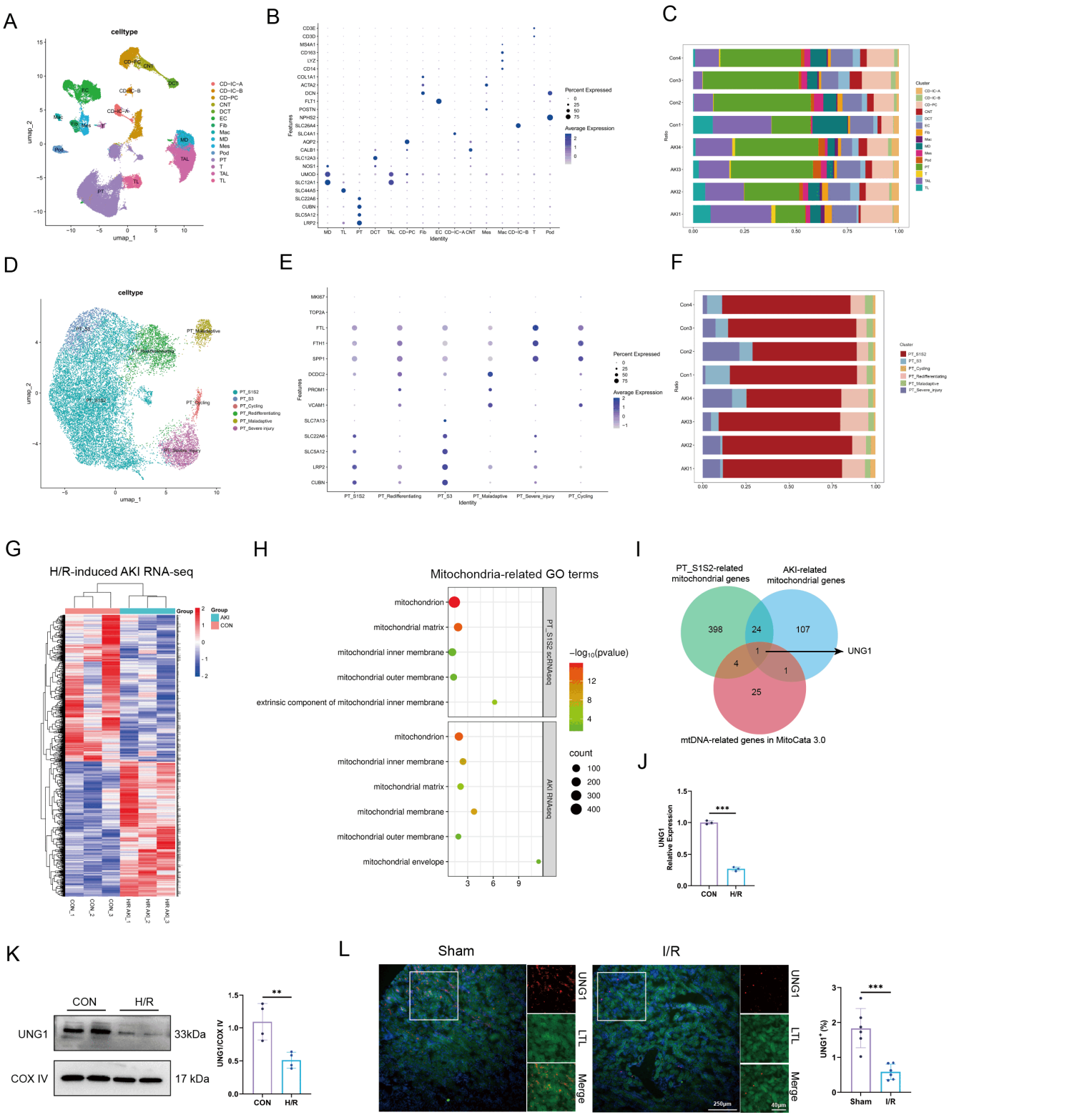


Figure 2

The mitochondrial protein UNG1 is downregulated in AKI. (A) Uniform manifold approximation and projection (UMAP) of 58,807 kidney epithelium, stroma, and immune cell nuclei. (B) Bubble map showing the mean expression of selected marker genes in 15 cell clusters. (C) Bar plots showing the proportion of cell clusters. (D) UMAP of PT subclusters. (E) Bubble map showing the mean expression of selected marker genes in six cell clusters. (F) Bar plots showing the proportion of cell clusters. (G) Heatmap

showing DEGs in the CON and AKI groups. (H) GO terms related to mitochondria of PT_S1S2 scRNAseq and AKI RNAseq. (I) Venn diagram showing PT_S1S2, AKI, and mtDNA-related genes. (J) Relative mRNA expression levels of UNG1 (n = 3). (K) Western blot analysis and quantification of mitochondrial UNG1 protein expression levels (n = 4). (L) Representative immunofluorescence images co-stained with UNG1 and LTL and quantification of UNG1 and LTL levels (scale bar = 250 μm left panel, scale bar = 40 μm right panel). *P < 0.05, **P < 0.01, ***P < 0.001.

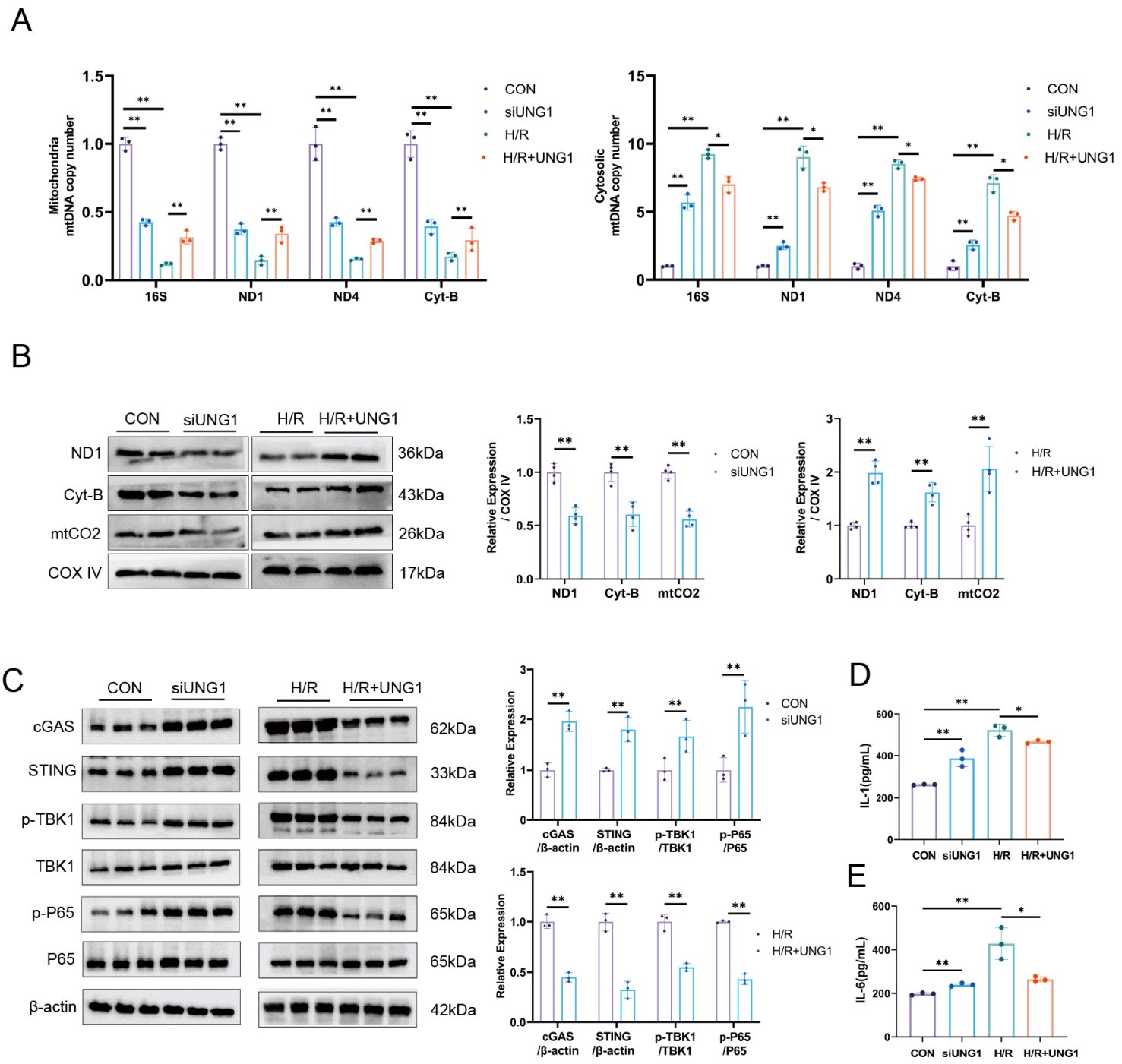


Figure 3

UNG1 mitigates the mtDNA-related cGAS-STING inflammatory response in H/R-induced AKI. (A) mtDNA copy number (16S, ND1, ND4 and Cyt-B) in the mitochondria and cytoplasm of HK-2 cells (n = 3). (B) Western blot analysis and quantification of ND1, Cyt-B and mtCO2 protein expression levels (n = 3). (C) Western blot analysis and quantification of components of the cGAS-STING pathway (n = 3). (D-E) IL-1 and IL-6 levels were detected in HK-2 cells by ELISA. *$P < 0.05$, **$P < 0.01$, ***$P < 0.001$.

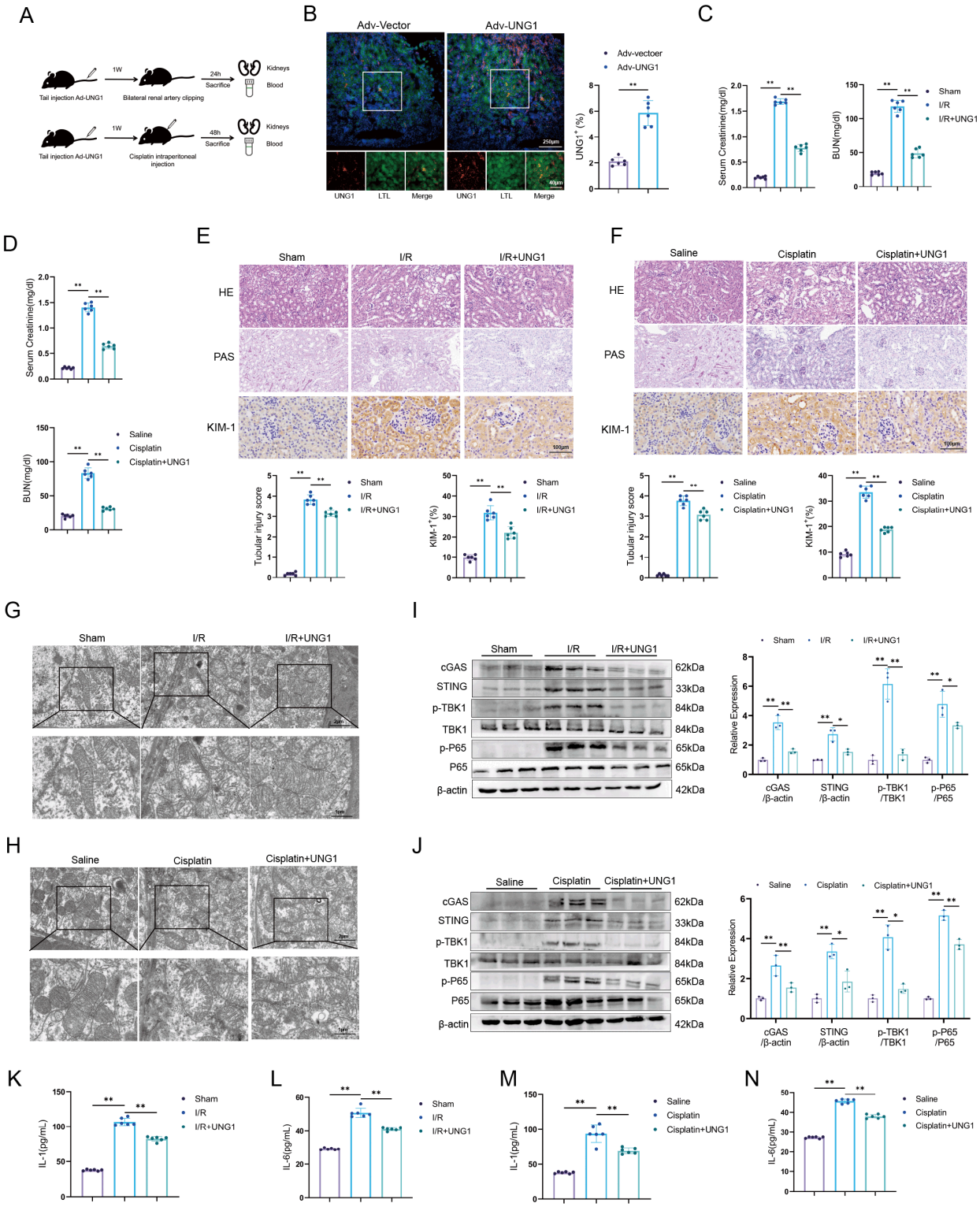
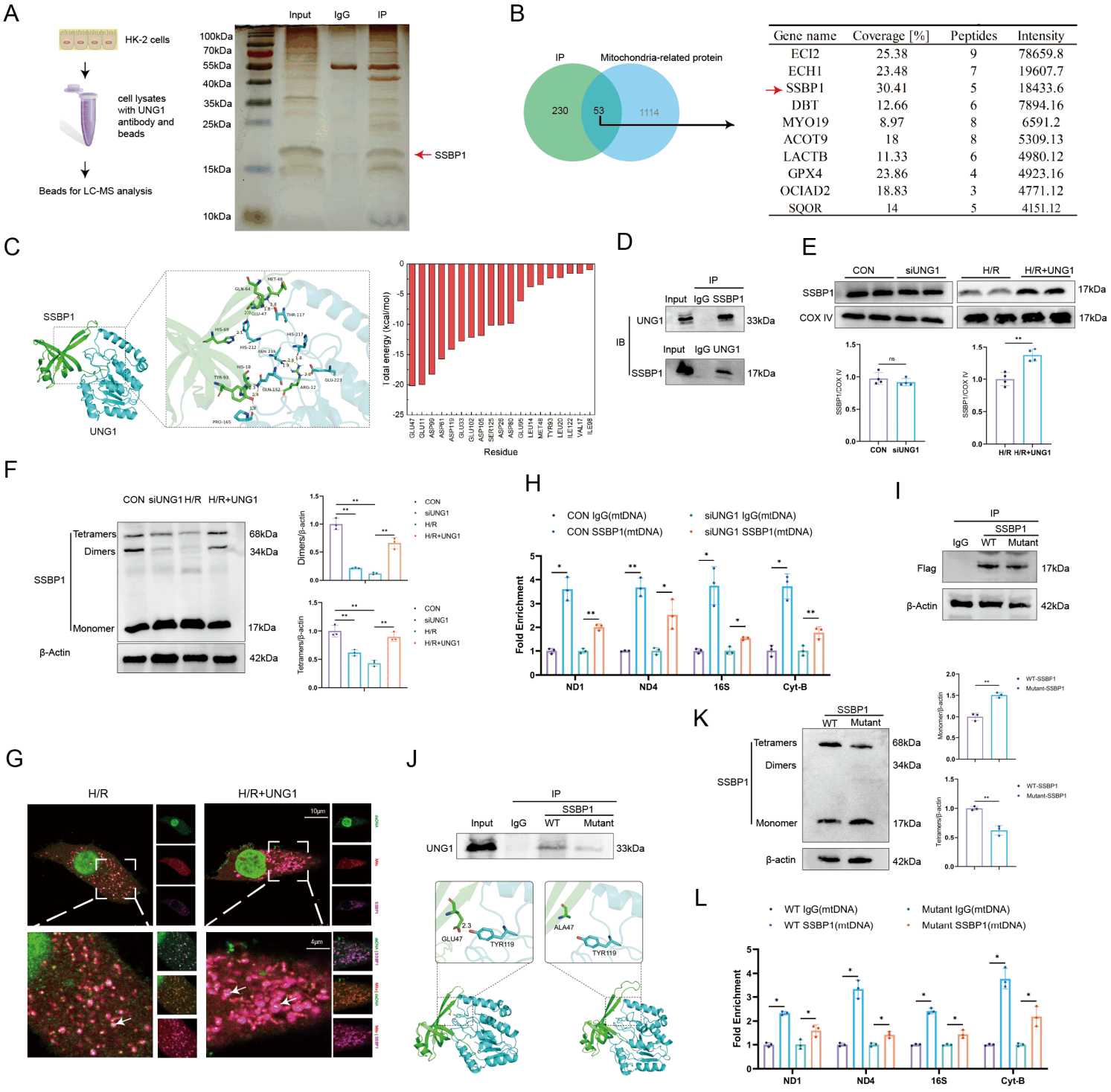


Figure 4

UNG1 protects kidney function in I/R- and cisplatin-induced AKI mice. (A) Schematic diagram showing the experimental design. (B) Representative immunofluorescence images co-stained with UNG1 and LTL and quantitative analysis of UNG1 and LTL levels (scale bar = 250 μm upper panel, scale bar = 40 μm lower panel). (C-D) Scr and BUN and levels in I/R- and cisplatin-induced AKI mice (n = 6). (E-F) H&E and PAS staining of kidney sections, and tubular injury score. Representative IHC images and quantitative analysis of KIM-1 staining (n = 6, scale bar = 100 μm). (G-H) Representative TEM images of kidney sections (scale bar = 2 μm upper panel, scale bar = 1 μm lower panel). (I-J) Western blot analysis and quantification of components of the cGAS-STING pathway (n = 3). (K-N) IL-1 and IL-6 levels were detected in mouse kidneys by ELISA. *P < 0.05, **P < 0.01, ***P < 0.001.



Gene name	Coverage [%]	Peptides	Intensity
ECI2	25.38	9	78659.8
ECH1	23.48	7	19607.7
→ SSBP1	30.41	5	18433.6
DBT	12.66	6	7894.16
MYO19	8.97	8	6591.2
ACOT9	18	8	5309.13
LACTB	11.33	6	4980.12
GPX4	23.86	4	4923.16
OCIAD2	18.83	3	4771.12
SQOR	14	5	4151.12

Figure 5

UNG1-mediated SSBP1 oligomerizationstabilizes mitochondrial nucleoids. (A) Schematic diagram showing the IP-mass spectrometry protocol and silver staining to show the enriched bands. (B) Venn diagram showing IP-specific and mitochondria-related proteins and the top10 proteins according to intensity. (C) Molecular docking of UNG1 and SSBP1, and binding free energy analysis of proteins in the ensemble. (D) Co-IP assay of UNG1 and SSBP1 interaction in HK-2 cells. (E) Western blot analysis and quantification of SSBP1 protein expression levels in the mitochondria (n = 4). (F) SSBP1 oligomerization analysis and quantification of dimers and tetramers in HK-2 cells (n = 3). (G) Representative

immunofluorescence images showing the co-staining of Mitotracker, SSBP1 and dsDNA (scale bar = 10 μm upper panel, scale bar = 4 μm lower panel), white arrows show co-localization. (H) The effects of UNG1 gene silencing on the enrichment of mtDNA (16S, ND1, ND4 and Cyt-B) fragments using anti-SSBP1 or IgG (negative control) to co-precipitate DNA (n = 3). (I) Co-IP with FLAG to verify expression of Mutant-SSBP1 in HK-2 cells. (J) Co-IP showing the interactions between UNG1 and WT-SSBP1 or Mutant-SSBP1, molecular docking of UNG1 and Mutant-SSBP1. (K) SSBP1 oligomerization analysis and quantification of monomer and tetramers in HK-2 cells (n = 3). (L) The effects of Mutant-SSBP1 on the enrichment of mtDNA (16S, ND1, ND4 and Cyt-B) fragments using anti-SSBP1 or IgG (negative control) to co-precipitate DNA (n = 3). *P < 0.05, **P < 0.01, ***P< 0.001.

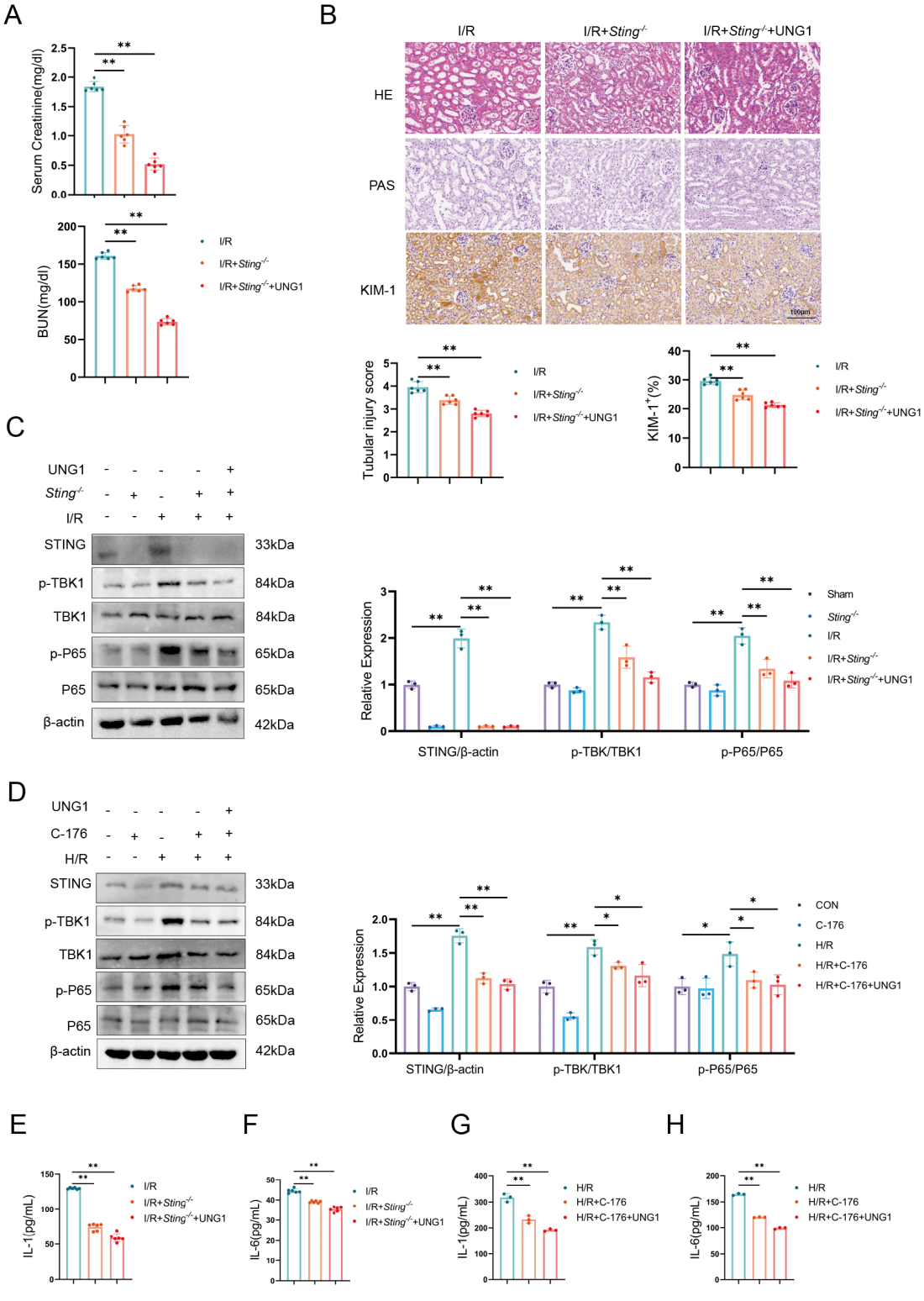


Figure 6

UNG1 attenuates renal inflammation in *Sting*$^{-/-}$ mice with AKI. (A) Scr and BUN levels in I/R-induced AKI models in *Sting*$^{-/-}$ mice (n = 6). (B) HH&E and PAS staining of kidney sections, and tubular injury score. Representative IHC images and quantitative analysis of KIM-1 staining (n = 6, scale bar = 100 μm) (n = 6, scale bar = 100 μm). (C-D) Western blot analysis and quantification of STING, TBK1, p-TBK1, P65 and p-

P65 protein expression levels in mouse kidneys and HK-2 cells (n = 3). (E-H) IL-1 and IL-6 levels were detected in mouse kidneys (n = 6) and HK-2 cells (n = 3) by ELISA. *P < 0.05, **P < 0.01, ***P < 0.001.

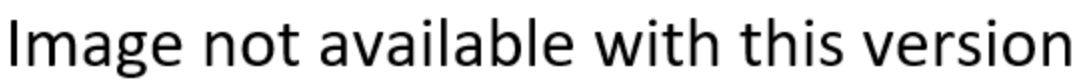


Figure 7

The mechanism diagram of UNG1 deficiency in AKI progression.

Supplementary Files

This is a list of supplementary files associated with this preprint. Click to download.

- Supplementarytable1.xlsx
- Supplementarytable3.xlsx
- Supplementarytable2.xlsx
- Fig3Supplementary.tif
- Westernblotrawdata.pdf
- Fig1Supplementary.tif
- Fig4Supplementary.tif
- Supplementarylegends.docx
- Fig2Supplementary.tif